

Designing Flat Bands and Pseudo-Landau Levels in GaAs with Patterned Gates

Pierre A. Pantaleón,^{1,*} Zhen Zhan,¹ S. Morales,² and Gerardo G. Naumis^{2,†}

¹*Imdea Nanoscience, Faraday 9, 28015 Madrid, Spain*

²*Depto. de Sistemas Complejos, Instituto de Física,*

Universidad Nacional Autónoma de México (UNAM). Apdo. Postal 20-364, 01000 México D.F., México

We investigate the electronic properties of two-dimensional electron gases (2DEGs) subjected to a periodic patterned gate. By incorporating the superlattice potential (SL) induced by patterning into the Schrödinger equation, we develop a methodology for obtaining exact analytical solutions. These solutions enable us to construct a comprehensive phase diagram illustrating the emergence of narrow bands and pseudo-Landau levels driven by the SL potential. To complement the analytical approach, we employ a standard plane-wave formalism to track the evolution of the band structure as the SL strength increases. Furthermore, we introduce a self-consistent Hartree screening to account for the interplay between the SL potential and electronic interactions. Our findings not only reveal a competition between SL strength and electron-electron interactions, leading to a reduction in the effective potential, but also highlight the value of exact analytical solutions for understanding and engineering electronic phases in patterned 2DEG systems.

I. INTRODUCTION

Many years ago, Albrecht et. al. investigated high mobility two-dimensional electron systems subjected to a periodic superlattice (SL) potential using GaAs heterojunctions [1]. In these systems, the electronic properties were found to be determined by the successive quantum wells rather than by the individual semiconductor layers [2]. More recently, the interest on such kind of systems has been revived in the context of emulating 2D materials and 2D moiré modulated materials in semiconductors [3, 4] and graphene heterostructures [5–8]. One of the primary motivations behind this revival is the potential to produce highly correlated many-body phases [9–11], similar to those observed in magic-angle twisted graphene [12–14]. As is well known, flat bands play a key role in enabling this behavior [15–17]. These flat bands are associated with pseudo-Landau levels [17–19] and can be considered as a form of topological solitons [20]. Here, we propose a strategy to achieve such flat bands in semiconductor heterostructures opening the possibility of doing superlattice engineering as in graphene systems [21–24].

In this work, by considering a two-dimensional electron gas placed on top of a patterned gate we derive exact analytical solutions describing the effects of a SL potential with triangular and square geometries. By providing a comprehensive phase diagram, we map the parameter space governing the emergence of narrow bands and pseudo-Landau levels. Additionally, by representing the Hamiltonian in a plane-wave basis, we track the evolution of the band structure as a function of the superlattice strength. Finally, by incorporating self-consistent Hartree screening, we reveal a competition between the SL potential strength and the screening effects.

The layout of this work is the following: in Sec. II we present the model of such structures and its electronic properties are discussed in Sec. III. Two important examples, the rectangular and square lattices are presented in Sec. III A while the hexagonal SL is presented in Sec. III D. Finally, the conclusions are given in Sec. VII.

II. MODEL

We consider a two-dimensional GaAs heterostructure subjected to the effect of a patterned gate [3]. As shown in Figure 1, the metallic lower patterned gate lays on the surface of a semiconductor. The voltage on the top gate creates anti-dots in the two-dimensional electron gas under the perforations in the lower gate. The combination of both gates create a periodic electrostatic potential, $U(\mathbf{r})$ [25]. As there is no charge density, the gate potential satisfies Laplace's equation. Expanding it by using a proper basis of functions for cylindrical coordinates $\mathbf{r} = (\rho, z)$, in this case the exponentials $e^{\pm\gamma z}$ in z and the complex exponentials $e^{i\mathbf{G}\cdot\rho}$ in ρ as the lattice is periodic. For a given z we can expand the harmonics in a reciprocal lattice basis $\mathbf{G} \in \Lambda^*$, while keeping the physical expansion in z , i.e. the negative exponential. Therefore, the most general gate potential can be written as,

$$U(\mathbf{r}) = \underbrace{-eEz}_{\text{boundary condition, } z \rightarrow \infty} + \sum_{\mathbf{G} \in \Lambda^*} \alpha_{\mathbf{G}} e^{-kz} e^{i\mathbf{G}\cdot\rho}. \quad (1)$$

We can further label the reciprocal lattice vectors \mathbf{G} in terms of a given basis $\{\mathbf{G}_1, \mathbf{G}_2\}$ defined by the periodicity of the SL potential, where $\mathbf{G} = \mathbf{G}_{mn} = m\mathbf{G}_1 + n\mathbf{G}_2$, and thus the potential is rewritten as,

$$U(\mathbf{r}) = -eEz + \sum_{mn} \alpha_{mn} e^{-G_{mn}z} \cos(\mathbf{G}_{mn} \cdot \rho). \quad (2)$$

We can set our coordinate system at the bottom of the perforated gate. Away from the gates, the harmonic part

* pierre.pantaleon@imdea.org

† naumis@fisica.unam.mx

of the potential is modulated by $\cos(\mathbf{G}_{mn} \cdot \rho)$, therefore we can neglect all terms with $k_{nm} > \min(|\mathbf{G}_i|)$, then

$$U(\mathbf{r}) \approx -eEz + \sum_{|m|,|n|\leq 1} \alpha_{mn} e^{-G_{mn}z} \cos(\mathbf{G}_{mn} \cdot \rho). \quad (3)$$

We will focus on regions close to the gates, thus the term eEz plays no role and $e^{-G_{mn}z} \approx 1$. Finally, by considering a symmetric lattice we can see that α_{nm} is the same for the first harmonics, let's call it W . Dropping the constant term we finally get

$$U(\mathbf{r}) \approx W \sum_{|m|,|n|=1} \cos(\mathbf{G}_{mn} \cdot \rho). \quad (4)$$

This results in a simplified model governed by an effective Hamiltonian in two dimensions which depends only on a single parameter W representing the amplitude of the applied potential, yet capturing the essential physics [6, 26]. The total Hamiltonian is written as

$$H = \frac{p^2}{2m^*} + U(\mathbf{r}), \quad (5)$$

where m^* is the electron effective mass in GaAs and now $\mathbf{r} = \rho = (x, y)$. By construction the SL potential is a smooth periodic function such that $U(\mathbf{r} + \mathbf{L}_1) = U(\mathbf{r} + \mathbf{L}_2) = U(\mathbf{r})$, with \mathbf{L}_1 and \mathbf{L}_2 primitive lattice vectors. For a triangular (or square) SL, the lattice period is given by $L_m = |\mathbf{L}_1| = |\mathbf{L}_2|$. The reciprocal lattice vectors satisfy $\mathbf{G}_i \cdot \mathbf{L}_j = 2\pi\delta_{ij}$. For a triangular SL, the corners of the SL Brillouin Zone (sBZ) are given by $\mathbf{G} = (1/3)(\mathbf{G}_1 + 2\mathbf{G}_2)$. For a rectangular or triangular lattice the SL potential is given by

$$U(\mathbf{r}) = 2W \sum_j \cos(\mathbf{G}_j \cdot \mathbf{r}). \quad (6)$$

We note that the simple form of the above SL potential has been successfully used to describe the even scalar contributions of hBN substrates acting in graphene monolayers [6, 27–29] and graphene bilayers [7, 30]. In the following section we will discuss the electronic properties derived from such a SL potential acting on a bidimensional electron gas.

III. ELECTRONIC PROPERTIES: QUASI-FREE ELECTRONS, FLAT BANDS AND PSEUDO-LANDAUI LEVELS

The electron dynamics is described by the Schrödinger equation,

$$-\frac{\nabla^2 \psi(\mathbf{r})}{2m^*} + U(\mathbf{r})\psi(\mathbf{r}) = E\psi(\mathbf{r}), \quad (7)$$

where the potential is given by Eq (6). Let us discuss how the solutions to Eq (7) contain two limiting cases depending on the adimensional parameter,

$$q_j^* = \frac{W}{\hbar^2 |\mathbf{G}_j|^2 / 2m^*}, \quad (8)$$

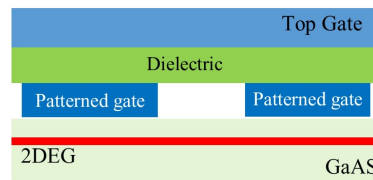


Figure 1. Schematics of a patterned gate acting on an GaAs heterostructure. The top gate modulates the strength of the potential and the patterned gate modulates the local charge density.

where $j = 1, 2$. This parameter measures the ratio between the maximal potential energy and maximal kinetic energy for electrons in the quasi-free electron approximation along the j direction. As detailed in the App A, for energies such that $E \approx q_j^* \ll 1$ the solutions are described within the free electron approximation and mimic the potential shape. For $E \approx q_j^* \gg 1$ and $W > 0$, the system behaves as a set of nearly isolated deformed quantum harmonic oscillator potentials centered at the minima (or maxima for $W < 0$) of $U(\mathbf{r})$. Mathematically, the reason is that for $q_j^* \gg 1$, the wave functions need big gradient envelopes to compensate for the strong potential energy. Although later on this will be explained in detail, in a neighborhood of the $U(\mathbf{r})$ minima, denoted generically as $\mathbf{r}_0 = (x_0, y_0)$, the potential can be approximated as,

$$U(\mathbf{r}) \approx U(\mathbf{r}_0) + \delta^T \mathcal{D}(\mathbf{r}_0) \delta \quad (9)$$

where $\delta^T = \mathbf{r} - \mathbf{r}_0$. $\mathcal{D}(\mathbf{r}_0)$ is the Hessian matrix evaluated at such extremal points,

$$\mathcal{D}(\mathbf{r}_0) = 2|W| \sum_j \begin{pmatrix} (\mathbf{G}_j^x)^2 & \mathbf{G}_j^x \mathbf{G}_j^y \\ \mathbf{G}_j^x \mathbf{G}_j^y & (\mathbf{G}_j^y)^2 \end{pmatrix}. \quad (10)$$

Due to the quadratic nature of Eq. (9), Landau levels will appear inside each minima basin producing flat-bands at low energies. Let us discuss below some examples of this behavior.

A. Rectangular and Square Lattices

Let's first consider a rectangular SL unit cell with dimensions L_1 and L_2 along the x and y axis respectively. We define the reciprocal vectors $\mathbf{G}_1 = (2\pi/L_1)(1, 0)$ and $\mathbf{G}_2 = (2\pi/L_2)(0, 1)$. The SL induced potential reads as:

$$U(\mathbf{r}) = 2W [\cos(G_1^x x) + \cos(G_2^y y)], \quad (11)$$

where $\mathbf{G}_j = (G_j^x, G_j^y)$. The corresponding Schrödinger equation $H\psi(\mathbf{r}) = E\psi(\mathbf{r})$, with E the energy and $\psi(\mathbf{r})$ the wave function, is separable into two ordinary second order differential equations by proposing a solution of the type $\psi(\mathbf{r}) = X(x)Y(y)$,

$$\frac{d^2 X(x)}{dx^2} + \frac{2m^*}{\hbar^2} (E_1 - 2W \cos(G_1^x x)) X(x) = 0, \quad (12)$$

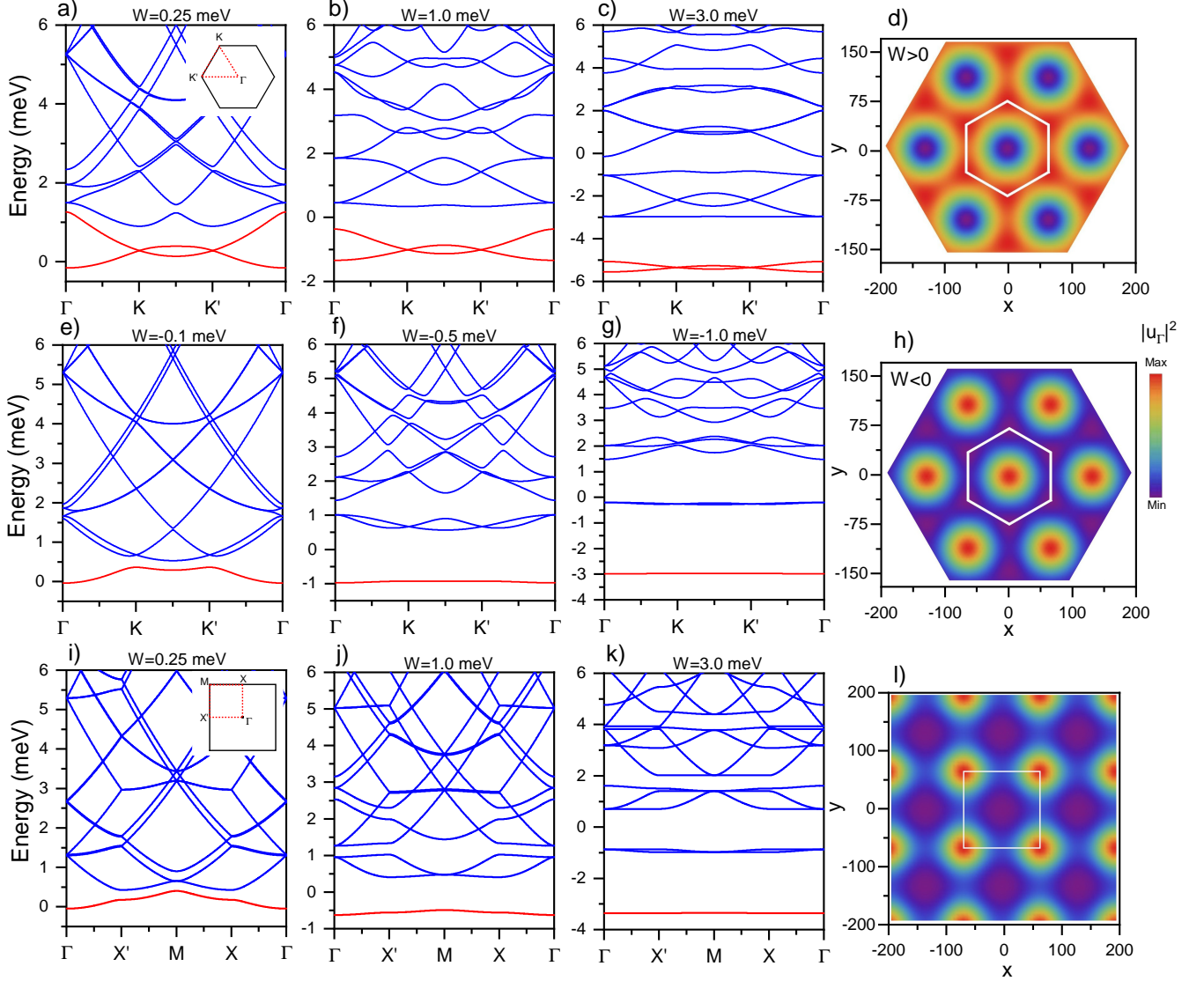


Figure 2. Electronic structure of GaAs subjected to a patterned SL potential. Top and middle rows are the bands with a triangular patterning and bottom row is for a square patterning. Red line are the lowest energy bands. Panels d), h) and i) are the electronic charge densities at the Γ point for the corresponding patterning. Our parameters are such that $E_0 = \hbar^2/2m^* = 0.56 \text{ eV nm}^2$, $m^* = 0.067m_e$, with m_e the electron mass and the SL length is set to $L = 130 \text{ nm}$. The high symmetry points and the evaluation paths are shown in a) and i). Observe how in c), g) and k) the lowest bands are almost flat reaching the Landau level limit. Also, the ground states in d), h) and i) resemble the $U(\mathbf{r})$ in agreement with Eq. (39).

$$\frac{d^2 Y(y)}{dy^2} + \frac{2m^*}{\hbar^2} (E_2 - 2W \cos(G_2^y y)) Y(y) = 0. \quad (13)$$

where $E = E_1 + E_2$. The previous equations are solvable using standard band theory techniques, i.e., by proposing Bloch wave solutions. In that case, E_1 and E_2 are functions of the wavevector $\mathbf{k} = (k_x, k_y)$. The resulting spectrum is seen in Fig. 2 for the cases $W = 0.25, 1.0$ and $W = 3.0 \text{ meV}$. Notice how the lower bands become flat as the confinement increases. To understand the details of how this happens, here we prefer to use a slightly different theoretical approach. This allows us to find analytical solutions for the wavefunctions. The trade-off is that the en-

ergy dispersion $E(\mathbf{k})$ is not straightforward. Nonetheless, the corresponding \mathbf{k} -values for the band edges are particularly easy to determine as they correspond to high-symmetry points in reciprocal space. Therefore, here we observe that Eq. (12) and Eq. (13) are Mathieu equations with the generic form,

$$\frac{d^2 \theta(t)}{dt^2} + [a - 2q \cos(2t)] \theta(t) = 0, \quad (14)$$

that are well known to describe a classical parametric driven pendulum, where $\theta(t)$ is the angular coordinate of the pendulum at time t . After a change of variables, Eq. (12) and Eq. (13) are written as a pair of Mathieu

equation with a set of different a, q parameters,

$$a_j = 8 \frac{m^* E_j}{\hbar^2 G_j^2}, \quad q_j = 16 \frac{m^* |W|}{\hbar^2 G_j^2}, \quad (15)$$

where $j = 1$ is used for Eq. (12) and $j = 2$ for Eq. (13). Notice that q_j is a refined version of the parameter q_j^* and basically represents the ratio between potential and kinetic quasi free particle energy. The solutions to the Mathieu equation are found using Floquet theory. They are linear combinations of the Mathieu cosine and sine functions, $ce(a, q, t)$ and $sn(a, q, t)$, respectively,

$$X(x) = A_{ce}^x ce(a_1, q_1, G_1^x x/2) + A_{sn}^x sn(a_1, q_1, G_1^x x/2), \quad (16a)$$

$$Y(y) = A_{ce}^y ce(a_2, q_2, G_2^y y/2) + A_{sn}^y sn(a_2, q_2, G_2^y y/2), \quad (16b)$$

which are equivalent to the Bloch solutions. Here $A_{ce}^x, A_{sn}^x, A_{ce}^y$ and A_{sn}^y are constants that depend on the boundary conditions. For example, symmetric solutions $X(-x) = X(x)$ require $A_{ce}^x = 1$ and $A_{sn}^x = 0$ while antisymmetric ones $X(-x) = -X(x)$ requires $A_{ce}^x = 0$ and $A_{sn}^x = 1$. The same is true for the y axis Mathieu equation.

B. Interpretation of the Stability Chart

The Mathieu equation presents bounded periodic solutions only for certain combinations of the parameters a and q [31]. The stability chart seen in Fig. 3 contains such information. Unstable solutions are associated with resonances between the fundamental frequency of the pendulum and the driving force $2q \cos(2t)$. For $q = 0$, the undriven harmonic oscillator is recovered corresponding to the undriven pendulum. This is equivalent to turning off the SL potential. Along the line where $a = 2q$, the amplitude of the cosine matches the undriven harmonic oscillator parameter. The stability condition in the Mathieu chart translates into allowed energies, i.e., unstable regions are spectral gaps while stable regions corresponds to the bands.

Here, the role of the pendulum is played by the free-particle solutions while the SL potential provides a spatial driving akin to the temporal driving. As seen in Fig. 3, for $q \ll 1$ the gaps are open at $a \approx n^2$ with $n = 1, 2, 3, \dots$, each corresponding to a resonance between the natural frequency of the pendulum and the frequency of the driving force. These gaps are translated here into a resonance between the spatial driving frequency $|G_j|$ and the wave vector component k_j . Physically, the gaps are open by diffraction as stationary waves are created by destructive or constructive interference whenever $k_j \approx nG_j$.

As we are dealing in our lattice problem with two equations, both a_1, q_1 and a_2, q_2 must lay in stable regions. Therefore, the Mathieu stability chart must be applied to

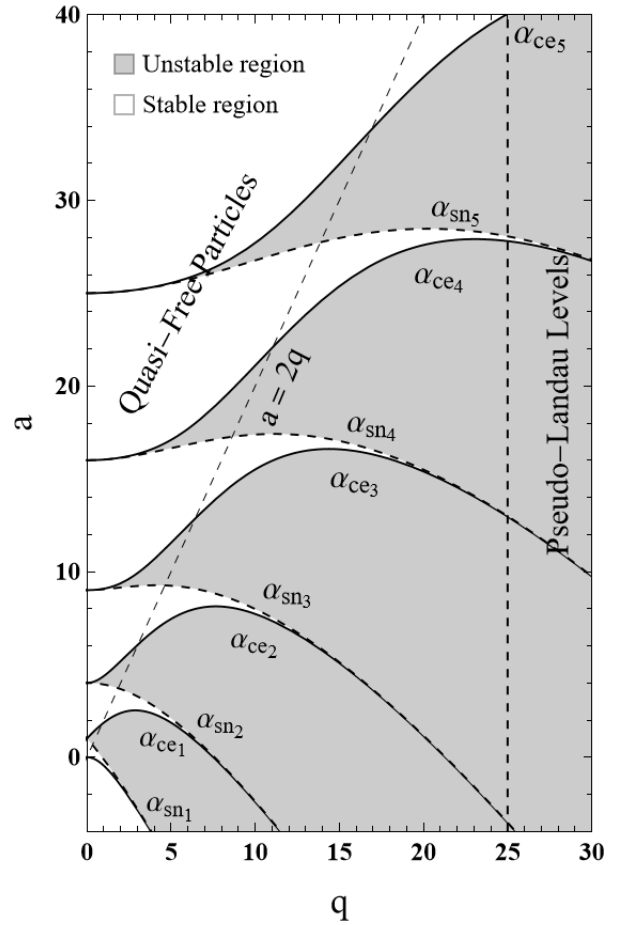


Figure 3. Mathieu equation stability chart, here corresponding to the eigenenergies of the square lattice on each direction. Stable regions correspond to bands while unstable regions are spectral gaps of the system. The solid and dashed curves, $\alpha_{ce}(q)$ and $\alpha_{sn}(q)$, stand for the eigenvalues of Mathieu's Floquet matrix corresponding to the eigenvectors (Mathieu functions) $ce(a, q, t)$ and $sn(a, q, t)$. The two different limiting regimes are highlighted with the transition line $a = 2q$, where the amplitude of the driven perturbation matches the undriven harmonic oscillator parameter. The vertical dotted line indicates how the spectrum is read for a given W , showing pseudo Landau levels at low energies. Only the $q \geq 0$ region is presented as the chart is the same for $q \leq 0$.

both the x and y directions. Since $E = E_1 + E_2$, the spectrum is degenerate as many combinations are possible for a single E . Also observe how q is fixed by W as indicated by a dotted vertical line in Fig. 3. The spectrum is read for a fixed W along such vertical line where each allowed value of a gives its corresponding energy. Each tongue in the Mathieu chart corresponds to a Bloch's energy band, and within each tongue, all possible \mathbf{k} values in one direction are considered. The pure Mathieu cosine and sine functions correspond to each of the band edges seen in Fig. 3, as they have periodic and antiperiodic boundary conditions. Also, observe that in Eq. (16), for a given combination of E_j and W in Eq. (15), the charge density

in real space appears to be obtained without requiring a Bloch representation. In fact, such a representation is embedded in the Mathieu functions and the stability chart, as both are calculated using a matrix determinant similar to Bloch's approach. However, this determinant can be analytically evaluated using a method developed by Whittaker [31], enabling the derivation of a closed-form solution.

C. Limiting Cases for the Rectangular Lattice

Now, let us discuss some limiting cases. Consider first the limit $2q_1 \gg a_1$ and $2q_2 \gg a_2$. In this case the driving force dominates. The solutions remain close to the minima of $\cos(2t)$. Therefore, the Mathieu equation reduces to the harmonic oscillator Schrödinger's equation and the corresponding wavefunctions are given by Landau level solutions [32],

$$X(x) = c_{n_1} H_{n_1} (2^{-3/4} q_1^{1/4} G_1^x x) e^{-\frac{1}{2} \sqrt{2q_1} \left(\frac{G_1^x x}{2}\right)^2}, \quad (17)$$

$$Y(y) = c_{n_2} H_{n_2} (2^{-3/4} q_2^{1/4} G_2^y y) e^{-\frac{1}{2} \sqrt{2q_2} \left(\frac{G_2^y y}{2}\right)^2}, \quad (18)$$

where c_{n_1}, c_{n_2} are two constants and $H_n(x)$ is a n -degree Hermite polynomial. The allowed parameters are,

$$a_j = 4\sqrt{q_j} \left(n_j + \frac{1}{2} \right) - 2q_j \quad (19)$$

with $n_j = 0, 1, 2, 3, \dots$. The resulting spectrum is akin to the Landau level spectrum,

$$E_{n_1, n_2} = \hbar\omega_1 \left(n_1 + \frac{1}{2} \right) + \hbar\omega_2 \left(n_2 + \frac{1}{2} \right) - 8W, \quad (20)$$

with frequencies,

$$\omega_j = 2G_j \left(\frac{W}{m^*} \right)^{1/2}. \quad (21)$$

Therefore, flat bands arise as the confinement increases due to the minima of the SL potential. The transition start to occur once $q_{1,2} > a_{1,2}/2$, i.e., for $E_1 < 16W$ and $E_2 < 16W$. Notice that for the square lattice, $G_1^x = G_2^y$ and $q_1 = q_2$, resulting in,

$$E_{n_1, n_2} = \hbar\omega_c (n_1 + n_2 + 1) - 8W, \quad (22)$$

where we defined an effective cyclotron frequency,

$$\omega_c \equiv 2G_1^x \left(\frac{W}{m^*} \right)^{1/2} = \frac{4\pi}{L} \left(\frac{W}{m^*} \right)^{1/2}, \quad (23)$$

with $L \equiv L_1 = L_2$. Such results are in agreement with the numerical spectrum seen in Fig. 2 for the cases $W = 0.25, 1.0$ and $W = 3.0$ meV. Therein, the confinement is strong for the lower bands. It is observed either

with a strong potential or a large lattice parameter, L . This partly explains why it has not yet been observed, as previous efforts have focused on smaller lattice parameters [1].

Let us discuss the other limit. For $q_1 = 0$ and $q_2 = 0$ all values of a_1 and a_2 are allowed and correspond to a continuous spectrum, a result to be expected due to the absence of a SL potential. The weak SL modulation case corresponds to $2q_1 \ll a_1$ and $2q_2 \ll a_2$. Gaps are open at,

$$a_j \approx n_j^2, \quad (24)$$

corresponding to the resonances of a weak perturbed parametric pendulum. In this case, the spectral gaps, i.e. resonances, are due to the induced SL diffraction as can be readily confirmed by using Eq. (24) and Eq. (15),

$$E_j = \frac{\hbar^2}{2m^*} \left(\frac{n_1 G_1^x}{2} \right)^2 = \frac{1}{2m^*} \left(\frac{n_1 P_1}{2} \right)^2, \quad (25)$$

showing that $n_1 G_1^x$ acts as a wave vector that opens a gap. As expected, in this limit the charge carriers behave as usual free particles under a weak periodic perturbation. We note that this weak coupling limit has been widely used to introduce triangular SL potentials in graphene heterostructures [6, 27–29, 33–35].

D. Hexagonal Superlattice

Now we will study a hexagonal SL, akin to the moiré effective potential that appears in twisted bilayer graphene [36]. When $W > 0$, the SL potential is repulsive in the origin and attractive at the edges of the unitary cell, the opposite is true for $W < 0$. The charge distribution of the ground state is localized in the attractive regions. Because of this, and as shown in Fig. 2d) and Fig. 2e) we can transform the system from an hexagonal to a triangular SL by only tuning the W value. Let us start with a triangular SL with spacing L_m . The SL is generated by the basis

$$\begin{aligned} \mathbf{G}_1 &= \frac{2\pi}{L} \left(1, -\frac{1}{\sqrt{3}} \right), \\ \mathbf{G}_2 &= \frac{4\pi}{L\sqrt{3}} (0, 1), \\ \mathbf{G}_3 &= \mathbf{G}_2 - \mathbf{G}_1, \end{aligned}$$

with $|\hat{\mathbf{G}}_j| \equiv G = 4\pi/\sqrt{3}L$. The SL is written as,

$$U(\mathbf{r}) = 2W \sum_{j=1}^3 \cos(\hat{\mathbf{G}}_j \cdot \mathbf{r}). \quad (26)$$

For $W > 0$, the minimum of the potential is $U = -3W$ and the maximum is $U = 6W$, such that the peak-to-peak potential amplitude U_{p-p} is $9W$. Let us simplify the

above expression by defining $u = \hat{\mathbf{G}}_1 \cdot \mathbf{r}$, $v = \hat{\mathbf{G}}_2 \cdot \mathbf{r}$, $w = \hat{\mathbf{G}}_3 \cdot \mathbf{r}$. Then we use triangular coordinates such that,

$$\begin{aligned}\zeta &= u + v, \\ \eta &= u - v.\end{aligned}$$

In triangular coordinates, the operator $\frac{p^2}{2m^*}$ is written as,

$$-\frac{\hbar^2 G^2}{2m^*} \left(\frac{\partial^2}{\partial \zeta^2} + 3 \frac{\partial^2}{\partial \eta^2} \right). \quad (27)$$

The potential is written as,

$$U(\zeta, \eta) = 2W \left[\cos \frac{\eta + \zeta}{2} + \cos \frac{\zeta - \eta}{2} + \cos \eta \right], \quad (28)$$

or

$$U(\zeta, \eta) = 2W \left[\cos \eta + 2 \cos \frac{\eta}{2} \cos \frac{\zeta}{2} \right]. \quad (29)$$

The advantage of the triangular coordinates is that the unitary cell is transformed into a rectangular domain defined by $0 \leq \eta \leq 2\pi$ and $0 \leq \zeta \leq 2\pi$. Also, such coordinates reflect in a natural way the symmetries of the triangular lattice unitary cell. In the minima of the potential, there is a strong confinement. Consider the case $W < 0$. The strong confinement occurs at the minima of the potential, i.e. around $\mathbf{r}_0 = 0$ and it implies that $\eta \ll 1$ and $\zeta \ll 1$, from where,

$$\begin{aligned}E\psi &= -\frac{\hbar^2 G^2}{2m^*} \left(\frac{\partial}{\partial \zeta^2} + 3 \frac{\partial}{\partial \eta^2} \right) \psi \\ &+ 2|W| \left[\frac{\zeta^2}{4} + \frac{3\eta^2}{4} - 3 \right] \psi.\end{aligned} \quad (30)$$

the previous equation can be separated resulting in two uncoupled quantum harmonic oscillators, i.e., using $\psi(\zeta, \eta) = \phi(\zeta)\chi(\eta)$ we have

$$-\frac{\hbar^2 G^2}{2m^*} \frac{\partial^2}{\partial \zeta^2} \phi + \frac{|W|}{2} \zeta^2 \phi = E_\zeta \phi, \quad (31)$$

$$-\frac{\hbar^2 G^2}{2m^*} \frac{\partial^2}{\partial \eta^2} \chi + \frac{|W|}{2} \eta^2 \chi = E_\eta \chi, \quad (32)$$

then we can write the total energy as a sum of harmonic oscillator energies,

$$E = \hbar\omega_1 \left(n_1 + \frac{1}{2} \right) + \hbar\omega_2 \left(n_2 + \frac{1}{2} \right) + E_0, \quad (33)$$

with

$$\omega_1 = \omega_2 = G \left(\frac{|W|}{m^*} \right)^{\frac{1}{2}} = \frac{4\pi}{\sqrt{3}L} \left(\frac{|W|}{m^*} \right)^{\frac{1}{2}}, \quad (34)$$

$$E_0 = -6|W|. \quad (35)$$

Notice again that although the original problem was not radial symmetric, the local confinement allows to have an

effective radial symmetric problem. Also, observe that the effective potential can be written as,

$$U_{\zeta, \eta} = -2|W| \left[2 \cos \frac{\eta}{2} \left(\cos \frac{\zeta}{2} + \cos \frac{\eta}{2} \right) - 1 \right], \quad (36)$$

and

$$U_{\zeta, \eta} = -2|W| \left[2 \sum_{s=0}^{\infty} \frac{(-1)^s}{2s!} \left(\frac{\eta}{2} \right)^{2s} \left(\cos \frac{\zeta}{2} + \cos \frac{\eta}{2} \right) - 1 \right]. \quad (37)$$

For $s = 0$ we recover a rectangular case, studied in the previous section. Higher orders in s increases the confinement in the η direction. A similar analysis can be made for $W > 0$ considering that the minima of the potential are no longer at $\mathbf{r}_0 = 0$.

IV. NATURE OF THE ELECTRONIC STATES

In twisted bilayer graphene, it is known that at the first magic angle, the electronic density of the flat-band states reproduces the shape of the potential [36]. For higher-order angles, these states take on a Gaussian profile with a pronounced tail [37]. More recently, it has been shown that the flat-band states are topological solitons that resemble Gaussians as a first approximation, a result similar to the heavy fermion model [38]. A similar phenomenology is observed here. Due to the Bloch's theorem, the electronic wave functions have the form,

$$\psi_{\mathbf{k}}(\mathbf{r}) = e^{\mathbf{k} \cdot \mathbf{r}} u_{\mathbf{k}}(\mathbf{r}), \quad (38)$$

For the quasi-free particle $q_j^* \ll 1$ limit, in the Appendix we prove that the ground state has the form,

$$\psi_{\Gamma}(\mathbf{r}) \approx C \left(1 + \frac{2m^*}{\hbar^2 |G|^2} (W - U(\mathbf{r})) \right), \quad (39)$$

where C is a normalization constant and we assumed that $|\mathbf{G}_j| = G$ for all j . Observe that from this we conclude that the ground state electronic density is proportional to the potential. Also notice how a change of sign in W is reflected in a change of the electronic density location. Figure 2d), Fig. 2h) and Fig. 2i) confirms the result given by Eq. (39), as the charge density at the Γ point tracks the potential with inverted sign. Such situation is akin to what happens for the first magic angle in twisted bilayer graphene [39]. In the case of strong confinement, the Landau level limit results as a boundary layer limit of the Schrödinger equation as shown in the App. A.

V. FOURIER SPACE REPRESENTATION

We now consider a general form by using a Fourier representation such that we expand in plane waves the SL potential. This procedure is akin to that introduced in

graphene monolayers with a triangular SL [26]. As before, we define a pair of reciprocal lattice vectors, \mathbf{G}_1 and \mathbf{G}_2 defined by the SL in the folded Brillouin zone. The momentum \mathbf{q} of the 2D electron gas is written into a momentum \mathbf{k} within the boundaries of the sBZ and a contribution from the SL. We define the momentum \mathbf{k} inside the sBZ such that:

$$\mathbf{q}_{mn} = \mathbf{k} + (m, n) \cdot (\mathbf{G}_1, \mathbf{G}_2) \equiv \mathbf{k} + \mathbf{G}_{mn}, \quad (40)$$

where $\mathbf{G}_{mn} = m\mathbf{G}_1 + n\mathbf{G}_2$ with m, n integers. For a triangular SL, each \mathbf{G}_{mn} vector has six nearest neighbors, where the \mathbf{G}_{mn} vectors with modulus $|\mathbf{G}_1|$, generate the so-called first harmonic functions [27]. Successive harmonics are further apart from the $\mathbf{G} = 0$ origin. By considering the SL potential as a perturbation, the low-energy electronic structure in a plane wave basis is written as

$$H = H_0(\mathbf{q}_{mn}) \otimes \mathbb{I}_N + \hat{V}_{SL}, \quad (41)$$

where H_0 is the Hamiltonian of a 2D electron gas with matrix elements,

$$[H_0(\mathbf{k})]_{mn} = \frac{\hbar^2}{2m^*} |\mathbf{k} + \mathbf{G}_{mn}|^2 \delta_{mn}. \quad (42)$$

Note that because δ_{mn} is the kronecker delta function, the above equation is diagonal in the plane wave basis. The potential \hat{V}_{SL} has matrix elements,

$$\left[\hat{V}_{SL} \right]_{mn} = W_j \delta_{\mathbf{G}_m - \mathbf{G}_n, \mathbf{G}_j}, \quad (43)$$

where for a triangular SL we set $W_j = W$ with \mathbf{G}_j the lattice vectors satisfying $|\mathbf{G}_j| = |\mathbf{G}_1|$. Finally, \mathbb{I}_N is an identity matrix with dimensions given by the number of reciprocal lattice vectors used in the calculations. To obtain the electronic structure the resulting matrix is diagonalized by truncating the number of reciprocal lattice vectors until convergence. This methodology has been widely used to determine the electronic properties of graphene multilayers and transition metal dichalcogenides placed on top of a patterned dielectric SL [5–8, 30, 40–43].

VI. ELECTROSTATIC INTERACTIONS

As shown in Fig. 2, increasing the amplitude W flattens the bands. The magnitude of this amplitude is determined by the gate voltages in the experimental setup [3]. In the low-energy bands, as the band dispersion decreases, the wavefunctions at different momenta become progressively more alike, leading to a self-screening effect [25]. As the bands are filled, their contribution to the charge density can be expressed in terms of a parameter ρ_G , which captures the symmetric and antisymmetric components of the charge density. The value of ρ_G depends on the wavefunction distribution in momentum space and can be computed self-consistently using a mean-field Hartree approximation.

Following Refs. [44, 45], this parameter is given by:

$$\rho_H(\mathbf{G}) = 2V_0(\mathbf{G}) \int \frac{d^2\mathbf{k}}{A_{\text{sBZ}}} \sum_{\mathbf{G}', l} \psi_{k,l}^\dagger(\mathbf{G}') \psi_{k,l}(\mathbf{G} + \mathbf{G}'), \quad (44)$$

where $V_0(\mathbf{G}) = v_C(\mathbf{G})/A_c$, with $v_C(\mathbf{G}) = 2\pi e^2/(\epsilon|\mathbf{G}|)$ is the Fourier transform of the Coulomb potential evaluated at \mathbf{G} , A_c is the area of superlattice unit cell, A_{sBZ} is the area of the superlattice Brillouin zone and l is a band index. $\psi_{k,l}$ are the eigenvectors resulting from the self-consistent diagonalization of the Hamiltonian in Eq. (41). The Hartree potential in real space is therefore given by

$$V_H(r) = 2 \sum_{mn} V_0(\mathbf{G}_{mn}) |\rho_H(\mathbf{G}_{mn})| \cos(\phi_{mn} + \mathbf{G}_{mn} \cdot r), \quad (45)$$

where $\phi_{mn} = \arg[\rho_H(\mathbf{G}_{mn})]$. The above equation implicitly depends on the filling fraction ν , with $\nu = 2$ for a full filled band. In addition, the variation of the charge density is such that $\rho_H(G, \nu) = \rho_0 + \delta\rho_H(G, \nu)$, we assume that $\rho_0 = 0$ at the bottom of the first band. In the low energy regions, the charge distribution is proportional to the SL potential but with a negative sign. This is illustrated in Fig. 2d)-h) and Fig. 2i) for triangular and square SL, respectively. Since the Fourier components of the Hartree potential in Eq. (44) are determined by integrating the charge distribution from charge neutrality to a given filling, the Hartree potential is also proportional to the SL potential. However, the Hartree screening opposes the SL strength, resulting in an effective potential $V_{\text{eff}} = V_{SL} + V_H$. This screening effect weakens the superlattice potential because, as W increases, more charge accumulates in the attractive regions, generating a repulsive potential in those areas such that V_{SL} and V_H have opposite signs. For example, by considering the triangular superlattice in Fig. 2c) where $W = 3.0$ meV. A Hartree correction with a filling fraction of $\nu = 1.1$ results in $\rho_G = -0.35$ and $V_H = -2.0$ meV. The effective potential is then $V_{\text{eff}} = 1.0$ meV which corresponds to the bands in Fig. 2b). It is important to mention that for the considered SL potentials only the vectors with $|G_{mn}| = |G_1|$ are required in Eq. (45), in addition, the Hartree screening generated by the low energy bands is a real number and therefore $\phi_{mn} = 0$. As the filling increases to the high energy bands the wavefunctions become too complex and additional Fourier components may be required [3, 24].

VII. CONCLUSIONS

In this work, we analyzed the effects of periodic SL potentials and electrostatic interactions on two-dimensional electron gases. By transforming the Schrödinger equation into ordinary second-order Mathieu equations, we derived exact analytical solutions describing the emergence of narrow bands and pseudo-Landau levels in 2DEGs under triangular and square SL potentials. Additionally,

we provided a comprehensive phase diagram for the electronic structure as a function of the superlattice strength and complemented our results with numerical analysis using standard Bloch wave techniques. By introducing a self-consistent Hartree potential, we uncovered a competition between the SL potential and screening effects, resulting in a reduction of the effective potential. This interplay offers a mechanism to control and fine-tune electronic band structures through external periodic potentials. These findings enhance our understanding of SL-modulated systems and pave the way for engineering novel electronic phases in 2DEGs.

ACKNOWLEDGEMENTS

We thank Francisco Guinea for discussions. This work was supported by CONAHCyT project 1564464 and UNAM DGAPA project IN101924. IMDEA Nanociencia acknowledges support from the ‘Severo Ochoa’ Programme for Centres of Excellence in R&D (CEX2020-001039-S/AEI/10.13039/501100011033).

P.A.P acknowledges support from NOVMOAT, project PID2022-142162NB-I00 funded by MICIU/AEI/10.13039/501100011033 and by FEDER, UE as well as financial support through the (MAD2D-CM)-MRR MATERIALES AVANZADOS-IMDEA-NC. Z.Z acknowledges support from the European Union’s Horizon 2020 research and innovation programme under the Marie-Sklodowska Curie grant agreement No 101034431.

Appendix A: Ground state

In this Appendix we show that the ground state is proportional to the potential whenever $q_j \ll 1$. Let’s consider Schrödinger’s equation with the Hamiltonian given by Eq. (5), and for simplicity, we discuss only the case $|\mathbf{G}_j| = G$. It can be written as,

$$-\frac{\nabla^2 \psi(\mathbf{r})}{|G|^2} + \alpha w(\mathbf{r})\psi(\mathbf{r}) = \epsilon \psi(\mathbf{r}) \quad (\text{A1})$$

where we defined the adimensional potential,

$$w(\mathbf{r}) = U(\mathbf{r})/W, \quad (\text{A2})$$

the effective strength interaction ratio,

$$\alpha = \frac{2m^*W}{\hbar^2|G|^2}, \quad (\text{A3})$$

and the adimensional energy,

$$\epsilon = \alpha = \frac{2m^*E}{\hbar^2|G|^2}. \quad (\text{A4})$$

Since the SL potential $U(\mathbf{r})$ is periodic in the lattice, then Bloch’s theorem tells us that the solution of Schrödinger’s equation is given by $\psi_{\mathbf{k}}(\mathbf{r}) = e^{i\mathbf{k}\cdot\mathbf{r}}u_{\mathbf{k}}(\mathbf{r})$, where \mathbf{k} is the crystal momentum vector and $u_{\mathbf{k}}(\mathbf{r})$ is a periodic function in the lattice. Now we take a perturbative expansion in the adimensional parameter α over the wave function $u_{\mathbf{k}}(\mathbf{r})$ and the adimensional energy $\epsilon_{\mathbf{k}}$, this is,

$$u_{\mathbf{k}}(\mathbf{r}) = \sum_{n=0} \alpha^n u_{\mathbf{k}}^{(n)}(\mathbf{r}), \quad (\text{A5})$$

$$\epsilon_{\mathbf{k}} = \sum_{n=0} \alpha^n \epsilon_{\mathbf{k}}^{(n)}, \quad (\text{A6})$$

where the index n represent the order in α . Since $u_{\mathbf{k}}(\mathbf{r})$ is periodic in the lattice, the functions $u_{\mathbf{k}}^{(n)}(\mathbf{r})$ are also periodic. Therefore, as they inherit the lattice periodicity we can Fourier expand them over the reciprocal lattice as

$$u_{\mathbf{k}}^{(n)}(\mathbf{r}) = \sum_{\mathbf{G} \in \Lambda^*} e^{i\mathbf{G}\cdot\mathbf{r}} S_{\mathbf{k}}^n(\mathbf{G}), \quad (\text{A7})$$

where $S_{\mathbf{k}}^n(\mathbf{G})$ are the coefficients to be determined from the Bloch equation. In this particular case, we are interested only in the ground state which is obtained for the Γ point, i.e., at $\mathbf{k} = (0, 0)$. Also, Eq. (A7) suggests that the wave function has a similar structure to $U(\mathbf{r})$. Thus it is natural to propose up to first order in α a wavefunction of the type,

$$\psi_{\Gamma}(\mathbf{r}) \approx 1 + \alpha[1 + \beta w(\mathbf{r})], \quad (\text{A8})$$

where β is a constant to be fixed. Using Eq. (A1), the zero order equation in α gives $\epsilon_{\Gamma}^{(0)} = 0$. By collecting the first order terms in α ,

$$(\beta + 1)w(\mathbf{r}) = \epsilon_{\Gamma}^{(1)}, \quad (\text{A9})$$

leading to $\epsilon_{\Gamma}^{(1)} = 0$ and $\beta = -1$. Finally,

$$\psi_{\Gamma}(\mathbf{r}) \approx C \left(1 + \frac{2m^*}{\hbar^2|G|^2} (W - U(\mathbf{r})) \right), \quad (\text{A10})$$

where C is set by normalization over the Brillouin zone. On the other hand, the limit $q_j \gg 1$ corresponds to $\alpha \rightarrow \infty$. In that case we can use a boundary layer theory approach, i.e., if the Laplacian term occurring in Eq. (A1) is neglected, this leads to $\psi_{\Gamma}(\mathbf{r}) = 0$ in most regions of the unitary cell. However, whenever

$$-\frac{\nabla^2 \psi(\mathbf{r})}{|G|^2} \sim \alpha, \quad (\text{A11})$$

the whole equation needs to be taken into account. As a result, states have amplitude mainly around the minima of $U(\mathbf{r})$, leading to the Landau level approach discussed before.

- [1] C. Albrecht, J. H. Smet, D. Weiss, K. von Klitzing, R. Hennig, M. Langenbuch, M. Suhrke, U. Rössler, V. Umansky, and H. Schweizer, *Phys. Rev. Lett.* **83**, 2234 (1999).
- [2] T. Duffield, R. Bhat, M. Koza, F. DeRosa, D. M. Hwang, P. Grabbe, and S. J. Allen, *Phys. Rev. Lett.* **56**, 2724 (1986).
- [3] D. Q. Wang, Z. Krix, O. A. Tkachenko, V. A. Tkachenko, C. Chen, I. Farrer, D. A. Ritchie, O. P. Sushkov, A. R. Hamilton, and O. Klochan, “Tuning the band-structure of electrons in a two-dimensional artificial electrostatic crystal in gaas quantum wells,” (2024), [arXiv:2402.12769](#).
- [4] D. Q. Wang, D. Reuter, A. D. Wieck, A. R. Hamilton, and O. Klochan, [arXiv \(2024\)](#), [arXiv:2403.07273](#).
- [5] T. Tan, A. P. Reddy, L. Fu, and T. Devakul, *Phys. Rev. Lett.* **133**, 206601 (2024).
- [6] Z. Zhan, Y. Li, and P. A. Pantaleon, [arXiv \(2024\)](#), [arXiv:2408.05272 \[cond-mat.mes-hall\]](#).
- [7] S. A. A. Ghorashi and J. Cano, *Physical Review B* **107** (2023), [10.1103/physrevb.107.195423](#).
- [8] S. A. A. Ghorashi, A. Dunbrack, A. Abouelkomsan, J. Sun, X. Du, and J. Cano, *Physical Review Letters* **130** (2023), [10.1103/physrevlett.130.196201](#).
- [9] A. V. Chubukov and S. A. Kivelson, *Phys. Rev. B* **96**, 174514 (2017).
- [10] P. Phillips, Y. Wan, I. Martin, S. Knysh, and D. Dalidovich, *Nature* **395**, 253–257 (1998).
- [11] S. Raghu and S. A. Kivelson, *Phys. Rev. B* **83**, 094518 (2011).
- [12] Y. Cao, V. Fatemi, S. Fang, K. Watanabe, T. Taniguchi, E. Kaxiras, and P. Jarillo-Herrero, *Nature* **556**, 43 (2018).
- [13] Y. Xie, A. T. Pierce, J. M. Park, D. E. Parker, E. Khalaf, P. Ledwith, Y. Cao, S. H. Lee, S. Chen, P. R. Forrester, K. Watanabe, T. Taniguchi, A. Vishwanath, P. Jarillo-Herrero, and A. Yacoby, *Nature* **600**, 439 (2021).
- [14] J. M. Park, Y. Cao, K. Watanabe, T. Taniguchi, and P. Jarillo-Herrero, *Nature* **590**, 249 (2021).
- [15] H. Tian, X. Gao, Y. Zhang, S. Che, T. Xu, P. Cheung, K. Watanabe, T. Taniguchi, M. Randeria, F. Zhang, C. N. Lau, and M. W. Bockrath, *Nature* **614**, 440–444 (2023).
- [16] S. A. Chen and K. T. Law, *Phys. Rev. Lett.* **132**, 026002 (2024).
- [17] J. Wang, J. Cano, A. J. Millis, Z. Liu, and B. Yang, *Phys. Rev. Lett.* **127**, 246403 (2021).
- [18] F. K. Popov and A. Milekhin, *Phys. Rev. B* **103**, 155150 (2021).
- [19] Y. Sheffer and A. Stern, *Phys. Rev. B* **104**, L121405 (2021), [arXiv:2106.10650 \[cond-mat.str-el\]](#).
- [20] E. Andrade, F. López-Urías, and G. G. Naumis, *Phys. Rev. B* **107**, 235143 (2023).
- [21] C. Forsythe, X. Zhou, K. Watanabe, T. Taniguchi, A. Pasupathy, P. Moon, M. Koshino, P. Kim, and C. R. Dean, *Nature Nanotechnology* **13**, 566–571 (2018).
- [22] R. Huber, M.-H. Liu, S.-C. Chen, M. Drienovsky, A. Sandner, K. Watanabe, T. Taniguchi, K. Richter, D. Weiss, and J. Eroms, *Nano Letters* **20**, 8046 (2020).
- [23] D. Barcons Ruiz, H. Herzig Sheinfux, R. Hoffmann, I. Torre, H. Agarwal, R. K. Kumar, L. Vistoli, T. Taniguchi, K. Watanabe, A. Bachtold, and F. H. L. Koppens, *Nature Communications* **13** (2022), [10.1038/s41467-022-34734-3](#).
- [24] S. Wang, Z. Zhan, X. Fan, Y. Li, P. A. Pantaleón, C. Ye, Z. He, L. Wei, L. Li, F. Guinea, S. Yuan, and C. Zeng, *Physical Review Letters* **133** (2024), [10.1103/physrevlett.133.066302](#).
- [25] O. A. Tkachenko, V. A. Tkachenko, I. S. Terekhov, and O. P. Sushkov, “Effects of coulomb screening and disorder on artificial graphene based on nanopatterned semiconductor,” (2014), [arXiv:1411.7440](#).
- [26] F. Guinea and T. Low, *Philosophical Transactions of the Royal Society A: Mathematical, Physical and Engineering Sciences* **368**, 5391–5402 (2010).
- [27] J. R. Wallbank, A. A. Patel, M. Mucha-Kruczyński, A. K. Geim, and V. I. Fal’Ko, *Physical Review B* **87**, 245408 (2013).
- [28] P. San-Jose, A. Gutiérrez-Rubio, M. Sturla, and F. Guinea, *Physical Review B* **90**, 075428 (2014).
- [29] J. Jung, A. M. Dasilva, A. H. Macdonald, and S. Adam, *Nature Communications* **6** (2015), [10.1038/ncomms7308](#), [arXiv:1403.0496](#).
- [30] Y. Zeng, T. M. R. Wolf, C. Huang, N. Wei, S. A. A. Ghorashi, A. H. MacDonald, and J. Cano, *Physical Review B* **109** (2024), [10.1103/physrevb.109.195406](#).
- [31] N. McLachlan, *Theory and Application of Mathieu Functions*, Dover books on engineering and engineering physics (Dover Publications, 1964).
- [32] S. A. Wilkinson, N. Vogt, D. S. Golubev, and J. H. Cole, *Physica E: Low-dimensional Systems and Nanostructures* **100**, 24 (2018).
- [33] M. Mucha-Kruczyński, J. R. Wallbank, and V. I. Fal’Ko, *Phys. Rev. B* **88**, 205418 (2013).
- [34] J. Jung, E. Laksono, A. M. Dasilva, A. H. Macdonald, M. Mucha-Kruczyński, and S. Adam, *Physical Review B* **96** (2017), [10.1103/PhysRevB.96.085442](#).
- [35] P. San-Jose, A. Gutiérrez-Rubio, M. Sturla, and F. Guinea, *Physical Review B* **90**, 115152 (2014).
- [36] P. San-Jose, J. González, and F. Guinea, *Phys. Rev. Lett.* **108**, 216802 (2012).
- [37] L. A. Navarro-Labastida, A. Espinosa-Champo, E. Aguilar-Mendez, and G. G. Naumis, *Phys. Rev. B* **105**, 115434 (2022).
- [38] Z.-D. Song and B. A. Bernevig, *Phys. Rev. Lett.* **129**, 047601 (2022).
- [39] L. Rademaker and P. Mellado, *Phys. Rev. B* **98**, 235158 (2018).
- [40] Z. E. Krix and O. P. Sushkov, *Physical Review B* **107** (2023), [10.1103/physrevb.107.165158](#).
- [41] J. Sun, S. A. A. Ghorashi, K. Watanabe, T. Taniguchi, F. Camino, J. Cano, and X. Du, [arXiv \(2023\)](#), [10.48550/ARXIV.2306.06848](#).
- [42] X.-C. Yang, H. Yu, and W. Yao, *Physical Review Letters* **128** (2022), [10.1103/physrevlett.128.217402](#).
- [43] L.-k. Shi, J. Ma, and J. C. W. Song, *2D Materials* **7**, 015028 (2019).
- [44] F. Guinea and N. R. Walet, *Proceedings of the National Academy of Sciences* **115**, 13174–13179 (2018).
- [45] T. Cea, N. R. Walet, and F. Guinea, *Physical Review B* **100** (2019), [10.1103/physrevb.100.205113](#).